Coupled translation-rotation eigenstates of H_2 in C_{60} and C_{70} on the spectroscopically optimized interaction potential: Effects of cage anisotropy on the energy level structure and assignments

Minzhong Xu,[1] Francesco Sebastianelli,[1] Brittney R. Gibbons,[1] Zlatko Bačić,[1,a)] Ronald Lawler,[2] and Nicholas J. Turro[3,b)]
[1]*Department of Chemistry, New York University, New York, New York 10003, USA*
[2]*Department of Chemistry, Brown University, Providence, Rhode Island 02912, USA*
[3]*Department of Chemistry, Columbia University, New York, New York 10027, USA*

(Received 27 April 2009; accepted 20 May 2009; published online 10 June 2009; publisher error corrected 12 June 2009)

We have developed a quantitatively accurate pairwise additive five-dimensional (5D) potential energy surface (PES) for H_2 in C_{60} through fitting to the recently published infrared (IR) spectroscopic measurements of this system for H_2 in the vibrationally excited $\nu=1$ state. The PES is based on the three-site H_2-C pair potential introduced in this work, which in addition to the usual Lennard-Jones (LJ) interaction sites on each H atom of H_2 has the third LJ interaction site located at the midpoint of the H–H bond. For the optimal values of the three adjustable parameters of the potential model, the fully coupled quantum 5D calculations on this additive PES reproduce the six translation-rotation (T-R) energy levels observed so far in the IR spectra of $H_2@C_{60}$ to within 0.6%. This is due in large part to the greatly improved description of the angular anisotropy of the H_2-fullerene interaction afforded by the three-site H_2-C pair potential. The same H_2-C pair potential spectroscopically optimized for $H_2@C_{60}$ was also used to construct the pairwise additive 5D PES of H_2 ($\nu=1$) in C_{70}. This PES, because of the lower symmetry of C_{70} (D_{5h}) relative to that of C_{60} (I_h), exhibits pronounced anisotropy with respect to the direction of the translational motion of H_2 away from the cage center, unlike that of H_2 in C_{60}. As a result, the T-R energy level structure of H_2 in C_{70} from the quantum 5D calculations on the optimized PES, the quantum numbers required for its assignment, and the degeneracy patterns which arise from the T-R coupling for translationally excited H_2 are all qualitatively different from those determined previously for $H_2@C_{60}$ [M. Xu *et al.*, J. Chem. Phys. **128**, 011101 (2008). © *2009 American Institute of Physics*. [DOI: 10.1063/1.3152574]

I. INTRODUCTION

The endohedral fullerenes $H_2@C_{60}$ (Refs. 1 and 2) and $(H_2)_n@C_{70}$ ($n=1,2$),[3] where one or two H_2 molecules are encapsulated inside the fullerene cages, have been synthesized recently utilizing the "molecular surgery" approach.[4] This has opened the way for the investigations of many facets of the fascinating dynamical behavior of the endohedral H_2 molecules. Nuclear magnetic resonance (NMR) spectroscopy has been used to probe the dynamical properties of H_2 in C_{60};[5–7] it has also revealed the positional exchange of two H_2 molecules trapped inside an open-cage C_{70}.[8] Various physical properties of H_2 in C_{60}, such as the quenching of $^1O_2$ outside the cage,[9] the spin-lattice relaxation rate,[10] and the interconversion of parahydrogen (p-H_2) and orthohydrogen (o-H_2),[11] have been studied as well in the last couple of years.

Much of the interest in the endohedral H_2-fullerene complexes stems from the realization that they provide an unparalleled opportunity to investigate the highly quantum dynamics of coupled translational and rotational motions of the guest hydrogen molecule(s) in nanoconfining geometries and how it is influenced by the symmetry of the environment. Confinement leads to the quantization of the three translational degrees of freedom of H_2 in addition to the two already quantized rotational degrees of freedom. Due to the small mass of H_2, HD, D_2, and their large rotational constants, the translation-rotation (T-R) energy level structure is rather sparse. For the homonuclear isotopomers H_2 and D_2 it is made even sparser by the symmetry constraints on the total wave function, as a result of which p- and o-H_2 have only even- and odd-j rotational states, respectively. Consequently, the T-R dynamics is highly quantum mechanical, especially at the very low temperatures at which many of the spectroscopic measurements discussed below are performed.

In addition, the quantum T-R dynamics is strongly influenced by the symmetry of the nanocage, which ultimately determines the patterns of the T-R energy levels and the translational quantum numbers appropriate for their assignment, the splittings of the rotational excitations, and the overall T-R coupling scheme. This was initially revealed by our theoretical studies of the T-R energy level structure of H_2 trapped inside the small[12,13] and large cages[14,15] of the structure II clathrate hydrates which, unlike the carbonaceous

a)Electronic mail: zlatko.bacic@nyu.edu.
b)Electronic mail: njt3@columbia.edu.

fullerenes, are formed by hydrogen-bonded water molecules. Despite their very different chemical nature, the fullerene and clathrate hydrate cages have comparable dimensions, if different in shapes and symmetries, so that confining hydrogen molecules in their interiors give rise to the same basic issues.

Therefore, it was only natural that subsequent to our investigations of the hydrogen hydrates,[12–15] and in the wake of the synthesis of $H_2@C_{60}$ (Refs. 1 and 2) and the experimental studies that followed,[5–11] we would turn our attention to the T-R dynamics of H_2 encapsulated in C_{60}. Our recent quantum five-dimensional (5D) calculations of the T-R eigenstates of $H_2@C_{60}$ (Ref. 16) (paper I), later extended to HD and D_2 (Ref. 17) (paper II), elucidated the salient features of the endohedral quantum T-R dynamics inside C_{60}, which turned out to be quite elegant. It was shown in depth in papers I and II that the T-R energy levels can be organized and assigned in terms of the quantum numbers n, l, j, and λ. In brief, the principal quantum number n of the three-dimensional (3D) isotropic harmonic oscillator (HO) ($n=0,1,2,\ldots$), together with the orbital angular momentum quantum number l ($l=n,n-2,\ldots,1$ or 0 for odd or even n, respectively), labels the translational excitations of the endohedral H_2, j is its rotational quantum number, and λ is the quantum number of the total angular momentum $\lambda=\mathbf{l}+\mathbf{j}$ with the values $l+j,l+j-1,\ldots,|l-j|$, which arises from the coupling of the translational and rotational degrees of freedom of the trapped H_2.

The calculations in papers I and II were performed on the intermolecular 5D potential energy surfaces (PESs) constructed by summing over the pairwise interactions of each atom of H_2 with each atom of C_{60}. The H–C pair interactions were modeled with the standard Lennard-Jones (LJ) 12-6 potential. This approach has been widely used to describe the interaction of H_2 with various form of carbon, e.g., single-walled carbon nanotubes (SWCNTs)[18–20] and graphite.[21] It is motivated by the fact that the H_2-nanocarbon interactions are primarily dispersive, and calculating a reliable endohedral 5D PES at a high level of *ab initio* electronic structure theory would be extremely time consuming. Unfortunately, the H_2-carbon potentials have not been characterized accurately in large part due to the scarcity of experimental data sensitive to them. Consequently, a range of H–C LJ parameters is available in the literature,[18,19] which give rise to PESs differing substantially in well depths and other important aspects. This is illustrated by Figs. 1(b) and 1(c), which show the one-dimensional (1D) cuts through two PESs of H_2 in C_{60}, utilized in papers I and II and denoted there as PES 1 and PES 2, respectively. These two PESs, generated using the LJ parameters taken from Ref. 19 and given in Table I, have very different well depths, shapes, and other properties which influence the T-R dynamics of the trapped H_2. Nevertheless, as pointed out in papers I and II, the quantum T-R dynamics of $H_2/HD/D_2$ in C_{60} on both PESs exhibit the same key features, showing that these are independent of the details of the interaction potentials, and thus robust and generic.

Still, the T-R energy levels computed on PES 1 and PES 2 with the same quantum numbers generally have very different excitation energies.[17] Which are closer to reality? We were not in a position to say with any confidence which of the two PESs provides a more accurate description of the interaction between H_2 and the interior of C_{60}. This would require comparison with spectroscopically measured T-R excitations, but none were available at the time when papers I and II were published. The situation changed recently with the publication of the infrared (IR) spectroscopic study of $H_2@C_{60}$.[22] The low-temperature IR spectra show six peaks

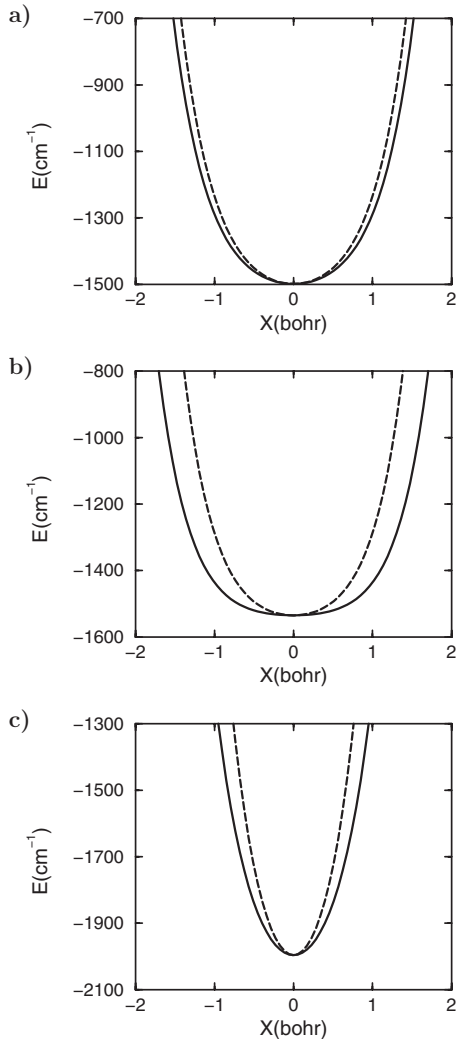

FIG. 1. 1D cuts through the three 5D interaction potentials of H_2 inside C_{60} employed in this work along a C_2 axis of C_{60} for H_2 perpendicular (full line) and parallel (dashed line) to the axis: (a) the optimized PES, (b) PES 1, and (c) PES 2.

TABLE I. Parameters specifying the PESs used in this work. ϵ (in cm^{-1}) and σ (in angstrom) are the LJ parameters and w, defined in the text, is dimensionless. For the optimized PES, ϵ, σ, and w are for H_2 in the vibrationally excited $v=1$ state obtained in this work by fitting to the IR spectroscopic measurements for $H_2@C_{60}$ (Ref. 22). The LJ parameters for PES 1 and PES 2 are from Refs. 17 and 19. For additional explanation, see the text.

Parameter	Optimized PES	PES 1	PES 2
ϵ(H–C)	2.99	18.0	19.2
σ(H–C)	2.95	2.78	3.08
w	7.5	⋯	⋯

which were assigned to the translational and rotational excitations of the endohedral H_2 molecule in the vibrationally excited $\nu=1$ state. The pattern of coupling between the translational and rotational modes inferred from the IR spectra[22] conformed to the theoretical predictions in papers I and II, validating the overall physical picture of the T-R dynamics of H_2 encapsulated in C_{60} which emerged from our work.

However, the energy of the translational fundamental calculated on PES 1 was lower, and that computed on PES 2 was higher than the experimental value. In addition, the splittings among the three $n=1$, $j=1$ energy levels of o-H_2 corresponding to $\lambda=1$, 2, and 0, respectively (in the order of increasing energies), calculated on both PESs, which are a measure of the T-R coupling, were larger than those observed in the IR spectra. This indicated that the T-R energy level structure computed on PES 1 and PES 2, although qualitatively correct in all essential aspects, is not quantitatively accurate. But now the IR spectra presented for the first time the opportunity to optimize the LJ parameters for the H–C pair potential on the basis of the set of experimental data which are highly sensitive to the interaction of H_2 with the C_{60} cage.

This paper consists of two interrelated parts. In the first part, we present the results of the optimization of the LJ parameters for the H–C interaction performed by varying their values until a very good match has been achieved between the T-R levels from the quantum 5D calculations of H_2 in C_{60} and those observed in the IR spectra of $H_2@C_{60}$.[22] The quantitative differences between our initial results computed on PES 1 and PES 2 in papers I and II and the IR spectroscopic data led Mamone *et al.*[22] to conclude that "it seems that the theory using a pairwise C–H potential is not accurate enough to describe the dynamics of $H_2@C_{60}$." The results discussed in this paper show otherwise; when the optimized LJ parameters are used for the six T-R energy levels observed in the IR spectra, the results obtained on the pairwise additive 5D PES of H_2 in C_{60} agree with the experimental values to better than 0.6%. But, such a high accuracy is achieved only after the introduction of the third LJ interaction site at the midpoint of the H–H bond in addition to the usual ones located on each H atom of H_2. We refer to this H_2–C two-body interaction as the three-site H_2–C pair potential. The excellent agreement with the experiment gives us reasons for confidence in the quantitative accuracy of the overall T-R energy level structure calculated on the optimized PES and its utility in the interpretation and assignment of the forthcoming more extensive higher-temperature IR spectroscopic data for $H_2@C_{60}$.[22]

In the second part of this paper, we report the results of the first quantum 5D calculations of the T-R eigenstates of H_2 in C_{70} on the pairwise additive PES constructed using the three-site H_2–C pair potential developed for $H_2@C_{60}$ above. The quantum dynamics of $H_2@C_{70}$ has not been previously investigated with any degree of rigor, either theoretically or experimentally. The symmetry of C_{70} (D_{5h}) is appreciably lower than that of C_{60} (I_h). Consequently, the profile of the interaction potential for the endohedral H_2 along the long axis of C_{70}, which coincides with the C_5 axis of rotation, is very different in both shape and spatial extent from the potential profiles along the two equivalent short axes of C_{70} perpendicular to the C_5 axis. The pronounced anisotropy of the endohedral PES with respect to the direction of the translational motion of the center of mass (cm) of H_2 inside C_{70} stands in sharp contrast to the very weak radial anisotropy of the interaction potential of H_2 in C_{60}.[16,17] The calculations presented in this paper show that the anisotropy of the C_{70} cage leads to the T-R energy level structure and quantum numbers for the assignment of the translational excitations which differ completely, not just quantitatively but also qualitatively, from those determined for H_2 inside C_{60} in papers I and II. These calculations for $H_2@C_{70}$ have a second objective, to enable the testing of the transferability of the three-site H_2–C pair potential optimized for H_2 in C_{60} to a different although related system, through comparison of the calculated T-R excitations with the experimental data from the IR spectroscopy, and possibly inelastic neutron scattering studies, of H_2 in C_{70}, which we hope will emerge soon.

II. THEORY

A. Calculations of the coupled translation-rotation eigenstates

The description of the theoretical approach employed in this work is available in paper I. This methodology was developed by us earlier for the purpose of calculating the T-R eigenstates of H_2 and isotopomers inside the cages of the clathrate hydrates.[12,13] The fullerenes, C_{60} and C_{70}, are treated as rigid, and their geometries used in our calculations have been determined experimentally from the gas-phase electron diffraction study of C_{60} (Ref. 23) and the neutron diffraction measurements of solid C_{70}.[24] The bond length of the endohedral molecule is also held fixed. The set of five coordinates (x,y,z,θ,ϕ) is employed; x, y, and z are the Cartesian coordinates of the cm of H_2, while the two polar angles θ and ϕ specify its orientation. The coordinate system is aligned with the three principal axes of the fullerene, and its origin is at the cm of the cage. The three rotational constants of C_{60}, a spherical top, are equal to 2.803×10^{-3} cm^{-1}, while C_{70} is a prolate symmetric top with one rotational constant of 2.261×10^{-3} cm^{-1} and the other two equal to 1.947×10^{-3} cm^{-1}. These very small rotational constants justify treating the fullerenes as nonrotating. In this case, the 5D Hamiltonian for the T-R motions of the caged diatomic molecule is

$$H=-\frac{\hbar^2}{2\mu}\left(\frac{\partial^2}{\partial x^2}+\frac{\partial^2}{\partial y^2}+\frac{\partial^2}{\partial z^2}\right)+B\mathbf{j}^2+V(x,y,z,\theta,\phi). \quad (1)$$

In Eq. (1), μ is the reduced mass of H_2 in C_{60} (2.0104 amu) or C_{70} (2.0112 amu) and $\mathbf{j}^2$ is the angular momentum operator of the diatomic. The mass of H_2 (2.0160 amu) could have been used instead of μ, since the difference between them is negligible for our purposes. B denotes the rotational constant of the endohedral molecule and will be discussed shortly. $V(x,y,z,\theta,\phi)$ in Eq. (1) is the 5D PES described below. The energy levels and wave functions of the Hamiltonian in Eq. (1) are obtained utilizing the efficient computational methodology developed in our group.[12,25] The final Hamiltonian matrix, its size drastically reduced by the sequential diagonal-

TABLE II. Comparison of the T-R energy levels (in cm^{-1}) of p-H_2 and o-H_2 (in the $\nu=1$ excited state) inside C_{60} from the IR spectroscopy (Ref. 22) and quantum 5D calculations on the optimized PES and the empirical PES 1 and PES 2. The parameters specifying the three PESs are listed in Table I. The T-R quantum numbers n, j, and λ are defined in the text. For p-H_2, the computed energies are relative to the T-R ground-state energy on the respective PES, and for the optimized PES they are given in Table III. For o-H_2, the calculated energies are relative to the lowest state (0,1,1) of o-H_2; on the optimized PES, the energies shown are obtained as the difference between the energy levels (n,j,λ) given in Table IV and the lowest state (0,1,1) at 109.63 cm^{-1}, also in Table IV. The numbers in brackets are the difference between the energy level next to it and the level above in the same column.

n	j	λ	Experiment		Optimized PES		PES 1		PES 2	
	p-H_2									
1	0	1	**183.6**		**183.5**		157.5		331.1	
1	2	1	**520.1**	(336.5)	**518.2**	(334.8)	503.4	(345.9)	697.2	(366.1)
	o-H_2									
1	1	1	**179.1**		**178.1**		141.9		307.6	
1	1	2	**185.3**	(6.2)	**184.6**	(6.5)	161.1	(19.1)	337.7	(30.1)
1	1	0	**195.6**	(10.3)	**194.9**	(10.3)	195.6	(34.5)	393.0	(55.3)
1	3	2	**737.1**		**737.2**					

ization and truncation procedure,[26] is diagonalized yielding the T-R eigenstates which are numerically exact for the 5D PES employed.

In the calculations reported here, in the case of $H_2@C_{60}$ the dimension of the sine-discrete variable representation (DVR) basis was 15 for each of the three Cartesian coordinates x, y, and z, and it spanned the range of -2.835 bohr $\leq\lambda\leq 2.835$ bohr $(\lambda=x,y,z)$. The angular basis included functions up to $j_{max}=7$. The energy cutoff parameter for the intermediate 3D eigenvector basis[25] was set to 4000 cm^{-1}, resulting in the final 5D Hamiltonian matrix of dimension 29 333. For $H_2@C_{70}$, the dimension of the sine-DVR basis was 15 in x and y coordinates and 20 for the z coordinate. Its ranges were -2.835 bohr$\leq\lambda\leq 2.835$ bohr $(\lambda=x,y,)$ and -3.779 bohr$\leq z\leq 3.779$ bohr. The angular basis also included functions up to $j_{max}=7$. With the energy cutoff parameter for the intermediate 3D eigenvector basis set to 3000 cm^{-1}, the dimension of the final 5D Hamiltonian matrix was 37 763.

B. Optimization of the 5D endohedral PES by fitting to the IR spectroscopy measurements for $H_2@C_{60}$: Introducing the three-site H_2-C pair potential

The 5D interaction potential $V_{H_2\text{-fullerene}}$ between the confined H_2 molecule and N carbon atoms of the fullerene ($N=60$ or 70 in this work), assumed to be pairwise additive, is written as

$$V_{H_2\text{-fullerene}}(\mathbf{q})=\sum_{k=1}^{N} V_{H_2\text{-C}}(\mathbf{q},\Xi_k), \tag{2}$$

where $\mathbf{q}$ are the coordinates (x,y,z,θ,ϕ) of the endohedral H_2 molecule defined above, $V_{H_2\text{-C}}$ is the pair interaction specified below between H_2 and a carbon atom of the fullerene, and the index k runs over all fullerene C atoms, whose coordinates Ξ_k are fixed.

In papers I and II, and to the best of our knowledge all other studies involving H_2 and various nanostructured carbon materials, the two-body potential $V_{H_2\text{-C}}$ in Eq. (2) is written as the sum of two H–C pair interactions each described by the standard LJ 12-6 potential (unless H_2 is treated as a spherical particle having a single LJ H–C interaction[27]),

$$V_{LJ}(r)=4\epsilon_{HC}\left[\left(\frac{\sigma_{HC}}{r}\right)^{12}-\left(\frac{\sigma_{HC}}{r}\right)^{6}\right], \tag{3}$$

where ϵ_{HC} is the well depth of the potential and σ_{HC} is related to its equilibrium distance r_e, as $r_e=2^{1/6}\sigma_{HC}$. We denote this H_2-C potential as the *two-site* pair potential $V_{H_2\text{-C},2s}$,

$$V_{H_2\text{-C},2s}(\mathbf{q},\Xi_k)=V_{LJ}(r_1)+V_{LJ}(r_2), \tag{4}$$

where r_1 and r_2 are the distances of the two H atoms of H_2 from the kth C atom of the fullerene. PES 1 and PES 2 employed in papers I and II, which are of the form given in Eq. (2), are constructed from such two-site H_2-C pair potentials whose LJ parameters are given in Table I.

The pairwise additive PES of H_2 in C_{60} generated by summing over the two-site H_2-C pair interactions in Eq. (4) contains two adjustable LJ parameters, ϵ_{HC} and σ_{HC} in Eq. (3), which in principle can be optimized by minimizing the differences between the calculated and observed T-R energy levels. Table II shows the comparison between the six T-R energy levels observed in the IR spectra of $H_2@C_{60}$ (Ref. 22) and those from the quantum 5D calculation on PES 1 and PES 2. The IR spectra correspond to H_2 in the $\nu=1$ vibrationally excited state. Therefore, in our calculations, the effective rotational constant of H_2 appropriate for the $\nu=1$ state, $B_1=54.83$ cm^{-1}, was employed. This value for B_1 was obtained using the experimentally determined[22] $B_e=59.3$ cm^{-1} and $\alpha_a=2.98$ cm^{-1}, as $B_1=B_e-1.5\alpha_e$. The T-R levels in Table II are assigned with the quantum numbers n,j and λ introduced in papers I and II and recapitulated in Sec. I.

A glance at Table II reveals a serious problem with the idea of optimizing the LJ parameters of the two-site H_2-C pair interaction by comparison with the experiment. As mentioned already in Sec. I, the translational fundamental $(n=1,\ j=0,\ \lambda=1)$ computed on PES 1, 157.5 cm^{-1}, is *lower* and that on PES 2, 331.1 cm^{-1}, is *higher* in energy than the experimental value of 183.6 cm^{-1}. At the same time, the splittings among the three $n=1,\ j=1$ energy levels of o-H_2 with $\lambda=1$, 2, and 0, respectively, calculated on *both* PESs,

TABLE III. T-R energy levels of p-H_2 ($\nu=1$) inside C_{60} (in cm^{-1}) from the quantum 5D calculations on the optimized PES. The excitation energies ΔE are relative to the T-R ground-state energy $E_0=-1257.16$ cm^{-1} and g denotes the degeneracy of the levels. $\langle R\rangle$ (in atomic unit) is the mean value of the distance between the cms of H_2 and C_{60}. The T-R levels are assigned the quantum numbers n, j, and λ defined in the text; $c(j)$ is the contribution of the dominant H_2 rotational basis function having the quantum number j to a T-R eigenstate. The values of l shown in the last column are those consistent with the given n. The pairs of closely spaced levels with $\lambda \geq 3$, whose energies are in italics, arise from the splitting of the $2\lambda+1$ level degeneracy by the crystal field of I_h symmetry of C_{60}.

i	ΔE	g	$\langle R\rangle$	n	j	λ	$c(j)$	l
0	0.00	**1**	0.70	0	0	**0**	0.999	0
1	183.47	**3**	0.87	1	0	**1**	0.999	1
2	328.63	**5**	0.70	0	2	**2**	0.993	0
3	382.87	**5**	0.99	2	0	**2**	0.991	2
4	409.38	**1**	0.96	2	0	**0**	0.997	0
5	507.01	**5**	0.87	1	2	**2**	0.999	1
6	*513.40*	**4**	0.87	1	2	**3**	0.991	1
7	*513.50*	**3**	0.87	1	2	**3**	0.991	1
8	518.22	**3**	0.86	1	2	**1**	0.996	1
9	*596.09*	**4**	1.09	3	0	**3**	0.988	3
10	*596.92*	**3**	1.09	3	0	**3**	0.987	3
11	638.21	**3**	1.05	3	0	**1**	0.992	1
12	*705.06*	**3**	1.00	2	2	**3**	0.999	2
13	*705.32*	**4**	0.99	2	2	**3**	0.999	2
14	707.14	**5**	0.99	2	2	**2**	0.999	0,2
15	*713.67*	**4**	0.99	2	2	**4**	0.989	2
16	*713.96*	**5**	0.99	2	2	**4**	0.988	2
17	717.78	**3**	0.99	2	2	**1**	0.999	2
18	724.07	**1**	0.98	2	2	**0**	0.993	2
19	741.23	**5**	0.96	2	2	**2**	0.994	0,2
20	*822.69*	**4**	1.17	4	0	**4**	0.985	4
21	*823.60*	**5**	1.17	4	0	**4**	0.985	4
22	879.05	**5**	1.13	4	0	**2**	0.986	2
23	902.81	**1**	1.11	4	0	**0**	0.987	0

are significantly *larger* than those observed in the IR spectra. This strongly suggests that it is *not* possible to find a set of LJ parameters for the two-site H_2–C pair which will result in a good fit to both the translational fundamental and the splittings of the λ sublevels. We varied the LJ parameters fairly extensively, and although it was not difficult to find values for which the calculations reproduced the measured translational fundamental, the computed splittings of the λ sublevels were always much larger than the measured values.

These findings raised the following questions: Does this failure signal that a *quantitatively* accurate PES for H_2 in C_{60} cannot be constructed in the pairwise additive fashion [Eq. (2)] by summing over the two-body H_2–C interactions? Or does the main fault lie with the standard two-site H_2–C pair potential $V_{H_2\text{–C},2s}$ in Eq. (4)? If the former is true, the only option left would be a high-level *ab initio* electronic structure calculation of the 5D PES and testing its accuracy by comparison of calculated and measured T-R excitations. Moreover, this would preclude the possibility of determining transferable and reliable H_2–C pair potentials applicable to a variety of H_2-nanocarbon systems. Therefore, we decided to explore whether a more flexible but still simple form of the H_2–C pair interaction can be found which would lead to an accurate pairwise additive PES.

The splittings among the λ sublevels, such as the three $n=1$, $j=1$ energy levels of o-H_2 with $\lambda=1$, 2, and 0 shown in Table II, reflect the strength of the T-R coupling. The fact that the calculated λ splittings are invariably greater than the experimental ones implies that PES 1, PES 2, and other pairwise additive PESs generated using the two-site H_2–C pair potential $V_{H_2\text{–C},2s}$ in Eq. (4) exhibit too large an anisotropy with respect to the angular orientation of H_2 in the cage. In the hindsight, it is not difficult to see why this is the case. The two-site H_2–C pair interaction effectively depicts H_2 as a dumbbell, which corresponds to the electron density being sharply localized on the H atoms with none in the region between the nuclei. In reality, the electron density in H_2 is distributed much more evenly with a significant accumulation in the internuclear region. Therefore the actual angular anisotropy of the interaction potential of H_2 with the interior of C_{60} is expected to be much smaller than that described by the two-site model of the H_2–C pair interaction.

The remedy for the deficiency of the standard two-site H_2–C pair potential which suggests itself naturally is to introduce the *third* LJ interaction site at the midpoint of the H–H bond. We will refer to this model as the *three-site* H_2–C pair potential. In order to keep the number of adjustable parameters to a minimum while making the model more flexible, we decided (a) that the LJ potentials involving all three sites on the H_2 molecule would have the *same* values of ϵ_{HC} and σ_{HC} and (b) to multiply the LJ potential originating at the midpoint of H_2 by a *weight factor* w. The latter allows

TABLE IV. T-R energy levels of o-H_2 (ν=1) inside C_{60} (in cm^{-1}) from the quantum 5D calculations on the optimized PES. The excitation energies ΔE are relative to the T-R ground-state energy of p-H_2 (ν=1), E_0 =−1257.16 cm^{-1}. Other symbols have the same meaning as in Table III.

i	ΔE	g	$\langle R \rangle$	n	j	λ	$c(j)$	l
1	109.63	**3**	0.70	0	1	**1**	0.999	0
2	287.72	**3**	0.87	1	1	**1**	0.999	1
3	294.23	**5**	0.87	1	1	**2**	0.999	1
4	304.55	**1**	0.86	1	1	**0**	0.999	1
5	484.48	**5**	1.00	2	1	**2**	0.999	2
6	*494.07*	**4**	0.99	2	1	**3**	0.998	2
7	*494.58*	**3**	0.99	2	1	**3**	0.998	2
8	496.10	**3**	0.98	2	1	**1**	0.999	0,2
9	524.21	**3**	0.95	2	1	**1**	0.999	0,2
10	*658.16*	**4**	0.70	0	3	**3**	0.999	0
11	*658.18*	**3**	0.70	0	3	**3**	0.999	0
12	*694.87*	**3**	1.10	3	1	**3**	0.999	3
13	*695.58*	**4**	1.10	3	1	**3**	0.999	3
14	*707.92*	**4**	1.09	3	1	**4**	0.995	3
15	*708.56*	**5**	1.09	3	1	**4**	0.995	3
16	710.38	**5**	1.08	3	1	**2**	0.999	1,3
17	737.80	**3**	1.05	3	1	**1**	0.999	1
18	754.49	**5**	1.04	3	1	**2**	0.993	1,3
19	770.39	**1**	1.03	3	1	**0**	0.998	1
20	*836.04*	**3**	0.87	1	3	**3**	0.999	1
21	*836.08*	**4**	0.87	1	3	**3**	0.999	1
22	*844.04*	**4**	0.86	1	3	**4**	0.996	1
23	*844.19*	**5**	0.86	1	3	**4**	0.995	1
24	846.87	**5**	0.86	1	3	**2**	0.994	1

us to effectively change the "shape" of H_2 seen by the C_{60} interior, and thereby the angular anisotropy of the interaction potential between the two entities. The three-site H_2−C pair potential, denoted as $V_{H_2\text{–}C,3s}$, can be written as

$$V_{H_2\text{–}C,3s}(\mathbf{q},\Xi_k) = V_{LJ}(r_1) + V_{LJ}(r_2) + wV_{LJ}(r_m), \tag{5}$$

where r_1 and r_2 have the same meaning as in Eq. (4), r_m is the distance between the midpoint of the H–H bond and the kth C atom of the fullerene, and V_{LJ} is given by Eq. (3). In terms of this new two-body H_2−C potential, the pairwise additive 5D PES $V_{H_2\text{-fullerene}}$ is expressed as

$$V_{H_2\text{-fullerene}}(\mathbf{q}) = \sum_{k=1}^{N} V_{H_2\text{–}C,3s}(\mathbf{q},\Xi_k), \tag{6}$$

where, as in Eq. (2), $\mathbf{q}$ and Ξ_k are the coordinates of H_2 and the kth C atom of the fullerene, respectively, and N is the number of carbon atoms.

The 5D PES given by Eq. (6) has *three* adjustable parameters: ϵ_{HC}, σ_{HC}, and the weight w. We searched this 3D parameter space rather carefully and the set of parameters which gave the best match between the calculated and observed T-R energy levels of H_2 (ν=1) in C_{60} is listed in Table I. The PES defined by these three parameters will be referred to simply as the optimized PES. The effective rotational constant of H_2, B_1=54.83 cm^{-1} was used again. It is evident from Table II that for these parameters, the optimized PES of Eq. (6) reproduces *all* six T-R energy levels observed in the IR spectra of $H_2@C_{60}$ to within 1−2 cm^{-1} (0.6%) or better. Thus, with the pairwise additive 5D PES based on the three-site H_2−C pair potential $V_{H_2\text{–}C,3s}$ in Eq. (5) it is possible to achieve an excellent simultaneous fit to the translational fundamental and the splittings of the λ sublevels, which could not be done when the two-site H_2−C pair interaction $V_{H_2\text{–}C,2s}$ in Eq. (4) is employed. Evidently, the introduction of the third LJ site at the midpoint of the H–H bond has accomplished precisely what we hoped for and corrected the deficiency of the two-site H_2−C potential model.

Figure 1(a) displays two 1D cuts along a C_2 axis of C_{60} through the optimized 5D PES of H_2 inside C_{60} generated using the three-site H_2−C pair potential and the parameters in Table I for H_2 perpendicular and parallel to the axis, respectively. Analogous 1D cuts through PES 1 and PES 2 are shown in Figs. 1(b) and 1(c). For each PES, the difference between the "perpendicular" and "parallel" potential profiles reflects the angular anisotropy of the interaction. It is clear that the optimal PES, which provides a superior fit to all available IR spectroscopic data for $H_2@C_{60}$, has a much smaller angular anisotropy than PES 1 and PES 2. Such a small angular anisotropy essential for reproducing the measured splittings of the λ sublevels could not be obtained using the two-site H_2−C pair potential (without sacrificing a good fit to some other T-R levels), the building block of PES 1 and PES 2.

We point out that the set of optimal parameters ϵ_{HC}, σ_{HC}, and w given in Table I for the three-site H_2−C pair potential should not be considered as completely unique. What we know is that this particular parameter set defines a 5D PES which reproduces fully and with high accuracy the recent spectroscopic measurements, not necessarily the PES. Sev-

eral other triplets of these parameters have been identified which yield almost as good an agreement with the published experimental results. Further differentiation between such multiple parameter sets requires additional spectroscopic data for comparison with the calculations.

III. RESULTS AND DISCUSSION

A. The T-R energy levels of $H_2@C_{60}$ calculated on the optimized 5D PES

The T-R energy levels from the quantum 5D calculations on the optimized PES are shown for p-$H_2@C_{60}$ in Table III and for o-$H_2@C_{60}$ in Table IV up to about 900 cm^{-1} above the ground state of the encapsulated p-H_2. In both instances H_2 is in the $\nu=1$ state. The quantum numbers and other quantities which appear in the two tables were defined earlier, and in more detail in papers I and II. Since the global minimum of the PES is at -1498.71 cm^{-1} and the T-R ground-state energy E_0 is equal to -1257.16 cm^{-1} for p-H_2, the zero-point energy (ZPE) of the T-R motions is 241.55 cm^{-1}.

The T-R energy level structure computed on the optimized PES, while much more accurate quantitatively than those obtained on PES 1 and PES 2, shares with them all of the key features identified in papers I and II: (i) the orbital angular momentum $\mathbf{l}$ of the cm of H_2 and the rotational angular momentum $\mathbf{j}$ of H_2 couple to give the total angular momentum $\lambda=\mathbf{l}+\mathbf{j}$, which ranges from $l+j$ to $|l-j|$ in steps of one; (ii) the integer values of l are those allowed for the quantum number n of the 3D isotropic HO ($l=n,n-2,\ldots,1$ or 0 for odd or even n, respectively); (iii) the T-R states having the same quantum numbers n and j are split into as many distinct levels as there are different values of λ, each with the degeneracy $2\lambda+1$; (iv) the translationally excited states are not harmonic since their energies depend not only on n but also on l; (v) j is a good quantum number for all T-R states of H_2 considered; (vi) the T-R levels with $\lambda=3$ and 4 appear as closely spaced pairs of levels with the degeneracies 3 and 4 for $\lambda=3$ and 4 and 5 for $\lambda=4$, a manifestation of the "crystal field" splitting by the icosahedral I_h environment of C_{60}.

The T-R levels in Tables III and IV will be helpful to the experimentalists in the interpretation and assignment of the IR spectra of H_2 in C_{60} recorded at higher temperatures, which should be available in the near future.[22] A larger number of T-R transitions present in the higher-T spectra will provide an additional stringent test of the optimized PES and the underlying three-site model of the H_2–C pair interaction.

B. The optimized 5D PES for H_2 in C_{70}

The three-site H_2–C pair potential in Eq. (5) with the optimized parameters ϵ_{HC}, σ_{HC}, and w given in Table I was used to construct the pairwise additive 5D PES [Eq. (6)] for H_2 ($\nu=1$) in C_{70}. Although these potential parameters have been optimized for $H_2@C_{60}$, we believe that the PES they generate for H_2 inside C_{70} is significantly more accurate than a PES that would be obtained using any of the LJ parameters in the literature. The 1D profiles of the 5D PES of $H_2@C_{70}$ in the direction of the long (z) molecular axis along the C_5 axis of rotation and the two equivalent short (x and y) axes aligned with the two principal axes of C_{70} perpendicular to the z axis are shown in Fig. 2. For each of the axes, three 1D cuts are displayed, one for H_2 parallel to the axis in question and two for H_2 oriented along the other two axes, in order to reveal the angular anisotropy of the PES. The potential cuts along x and y axes shown in Figs. 2(b) and 2(c) are similar to that for $H_2@C_{60}$ in Fig. 1(a). But the 1D potential profile along the z axis shown in Fig. 2(a) is qualitatively different; it is highly anharmonic and almost flat over an extended central region of C_{70} with two symmetrically equivalent shallow minima, and it gives the H_2 molecule considerably more room to move than is possible in the x and y directions for a given excitation energy. Thus, the 5D PES of H_2 in C_{70} shows a pronounced anisotropy with respect to the direction, z versus x and y, in which the cm of H_2 moves away from the center of the cage in contrast to the PES of $H_2@C_{60}$ whose directional or radial anisotropy is very weak.

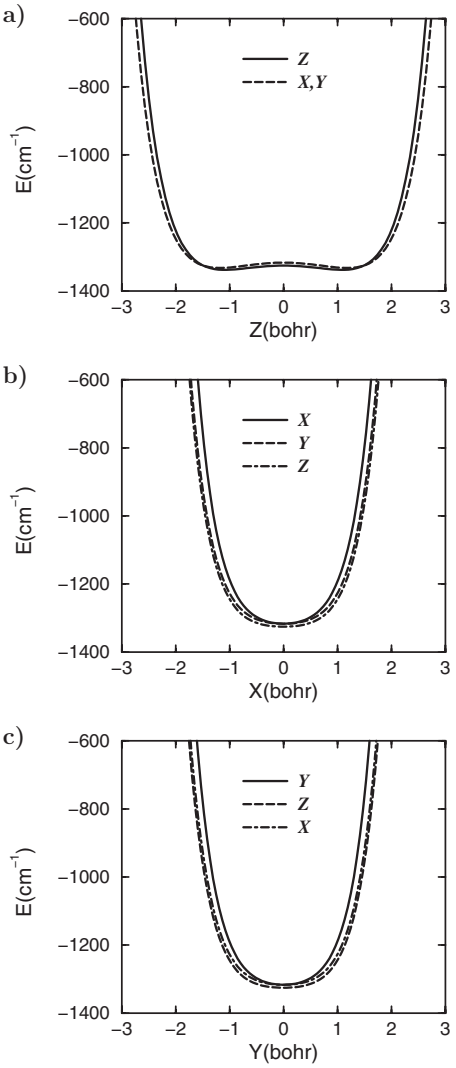

FIG. 2. 1D cuts through the optimized 5D PES of H_2 inside C_{70} employed in this work: (a) along the long (z) axis of C_{70} for H_2 parallel to the axis (full line) and parallel to the two short (x,y) axes (dashed line); (b) along the x axis for H_2 parallel to the axis (full line) and parallel to the y axis (dashed line) and the z axis (dashed-dot line); (c) along the y axis for H_2 parallel to the axis (full line) and parallel to the z axis (dashed line) and the x axis (dashed-dot line).

TABLE V. T-R energy levels of p-H_2 (ν=1) inside C_{70} (in cm^{-1}) from the quantum 5D calculations on the optimized PES. The excitation energies ΔE are relative to the T-R ground-state energy E_0=−1192.21 cm^{-1} and g denotes the degeneracy of the levels. Also shown are the rms amplitudes Δx, Δy, and Δz (in bohr). The translational quantum numbers $(v,|l|,v_z)$ are defined in the text; j is the quantum number of the dominant H_2 rotational basis function and $c(j)$ is its contribution.

i	ΔE	g	Δx	Δy	Δz	$(v,\|l\|,v_z)$	j	$c(j)$
0	0.00	1	0.46	0.46	0.74	(0,0,0)	0	0.999
1	54.15	1	0.44	0.44	1.14	(0,0,1)	0	0.999
2	131.87	1	0.43	0.43	1.30	(0,0,2)	0	0.999
3	138.74	2	0.60	0.65	0.67	(1,1,0)	0	0.998
4	205.63	2	0.57	0.63	1.06	(1,1,1)	0	0.998
5	224.93	1	0.43	0.43	1.42	(0,0,3)	0	0.999
6	292.11	2	0.56	0.61	1.24	(1,1,2)	0	0.997
7	293.45	2	0.72	0.72	0.62	(2,2,0)	0	0.986
8	314.27	1	0.68	0.68	0.63	(2,0,0)	0	0.892
9	327.06	**1**	0.49	0.49	0.74	**(0,0,0)**	**2**	0.879
10	327.24	**2**	0.46	0.46	0.74	**(0,0,0)**	**2**	0.999
11	331.30	1	0.43	0.43	1.50	(0,0,4)	0	0.982
12	333.06	**2**	0.46	0.46	0.74	**(0,0,0)**	**2**	0.989
13	370.53	2	0.69	0.69	1.01	(2,2,1)	0	0.928
14	379.84	**1**	0.47	0.47	1.12	**(0,0,1)**	**2**	0.938
15	381.93	**2**	0.44	0.44	1.13	**(0,0,1)**	**2**	0.998
16	386.93	**2**	0.46	0.46	1.14	**(0,0,1)**	**2**	0.932
17	392.83	2	0.59	0.57	1.38	(1,1,3)	0	0.993
18	394.25	1	0.66	0.66	1.01	(2,0,1)	0	0.933

C. The T-R dynamics of H_2@C_{70} on the optimized 5D PES: Energy level structure and quantum number assignment

The T-R energy levels from the quantum 5D calculations on the optimized PES described above are shown for p-H_2@C_{70} in Table V and for o-H_2@C_{70} in Tables VI–VIII together with their degeneracies. Since the parameters of the three-site H_2–C pair interaction in Table I are based on the IR spectra of H_2 (ν=1), for consistency the effective rotational constant B_1=54.83 cm^{-1} was used in the calculations. This rotational constant was determined experimentally for H_2 (ν=1) in C_{60}.[22] Nevertheless, it is certainly more appropriate for H_2 (ν=1) inside C_{70} than the gas-phase value for H_2 in the ν=1 state, 56.26 cm^{-1}. Therefore, the T-R energy levels given in Tables V–VIII pertain to H_2 (ν=1). For each state, the root-mean-square (rms) amplitudes Δx, Δy, and Δz are shown, which measure the wave function delocalization along the respective Cartesian coordinates and are helpful in making the quantum number assignments. Also given for each T-R eigenstate is the contribution $c(j)$ of the dominant rotational basis function j, determined as described in papers I and II. Since the values of $c(j)$ are generally greater than 0.9, j is a good quantum number for all the T-R states investigated. The global minimum of the PES lies at −1337.95 cm^{-1} and the T-R ground-state energy E_0 is −1192.21 cm^{-1}. Therefore the ZPE associated with the T-R modes is 145.74 cm^{-1}, considerably less than the ZPE of 241.55 cm^{-1} calculated for H_2@C_{60}.

1. Translational excitations

Even a cursory comparison of the T-R energy level structure of H_2@C_{70} (e.g., Table V), the degeneracy pattern, in

TABLE VI. T-R energy levels of o-H_2 (ν=1) inside C_{70} (in cm^{-1}) with *zero* quantum in the 2D translational (xy) mode perpendicular to the long (z) axis of C_{70} from the quantum 5D calculations on the optimized PES. The excitation energies ΔE are relative to the T-R ground-state energy E_0=−1192.21 cm^{-1}. Other symbols have the same meaning as in Table V.

i	ΔE	g	Δx	Δy	Δz	$(v,\|l\|,v_z)$	j	$c(j)$
1	104.77	**1**	0.47	0.47	0.73	**(0,0,0)**	1	0.999
2	112.14	**2**	0.46	0.46	0.74	**(0,0,0)**	1	0.999
3	160.05	**1**	0.45	0.45	1.13	**(0,0,1)**	1	0.999
4	165.63	**2**	0.44	0.44	1.14	**(0,0,1)**	1	0.999
5	238.88	**1**	0.44	0.44	1.29	**(0,0,2)**	1	0.999
6	242.70	**2**	0.43	0.43	1.30	**(0,0,2)**	1	0.999
7	333.23	**1**	0.44	0.44	1.41	**(0,0,3)**	1	0.999
8	335.06	**2**	0.43	0.43	1.42	**(0,0,3)**	1	0.999
9	440.64	**2**	0.43	0.43	1.52	**(0,0,4)**	1	0.999
10	440.96	**1**	0.43	0.43	1.50	**(0,0,4)**	1	0.999

TABLE VII. T-R energy levels of o-H_2 (v=1) inside C_{70} (in cm^{-1}) with *one* quantum in the 2D translational (xy) mode perpendicular to the long (z) axis of C_{70} from the quantum 5D calculations on the optimized PES. The excitation energies ΔE are relative to the T-R ground-state energy E_0=−1192.21 cm^{-1}. Other symbols have the same meaning as in Table V.

i	ΔE	g	Δx	Δy	Δz	$(v,\|l\|,v_z)$	j	$c(j)$
1	240.54	**2**	0.57	0.68	0.66	**(1,1,0)**	1	0.999
2	246.46	**1**	0.62	0.62	0.67	**(1,1,0)**	1	0.999
3	252.53	**2**	0.62	0.62	0.67	**(1,1,0)**	1	0.999
4	259.00	**1**	0.61	0.61	0.67	**(1,1,0)**	1	0.999
5	308.64	**2**	0.56	0.64	1.05	**(1,1,1)**	1	0.999
6	312.68	**1**	0.60	0.60	1.06	**(1,1,1)**	1	0.999
7	318.76	**2**	0.60	0.60	1.06	**(1,1,1)**	1	0.999
8	325.46	**1**	0.59	0.59	1.06	**(1,1,1)**	1	0.999
9	396.37	**2**	0.55	0.63	1.24	**(1,1,2)**	1	0.999
10	398.54	**1**	0.59	0.59	1.25	**(1,1,2)**	1	0.999
11	404.59	**2**	0.59	0.59	1.25	**(1,1,2)**	1	0.999
12	411.56	**1**	0.58	0.28	1.25	**(1,1,2)**	1	0.999

particular with that of H_2 in C_{60} (e.g., Table III), leads to the conclusion that the two are qualitatively different. Consequently, the quantum numbers of the 3D isotropic HO and the entire T-R coupling scheme used for H_2 in C_{60} do not apply to H_2 confined inside C_{70}. The clue to the quantum number assignment scheme appropriate for $H_2@C_{70}$ is provided by Figs. 3–7, which for the translationally excited (j=0) T-R eigenstates in Table V show the 3D reduced probability density (RPD) $\rho_i(x,y,z)$ in the translational (Cartesian) coordinates[12]

$$\rho_i(x,y,z) = \int \psi_i^*(x,y,z,\theta,\phi)\psi_i(x,y,z,\theta,\phi)\sin\theta d\theta d\phi, \quad (7)$$

where $\psi_i(x,y,z,\theta,\phi)$ is the ith T-R eigenfunction of the encapsulated p-H_2 or o-H_2.

The RPDs in Fig. 3 reveal a well defined quasi-1D translational mode along the z axis. The strikingly regular nodal pattern of the z-mode excitations suggests their weak coupling to the excitations in the xy plane. It also allows a straightforward assignment of the z-mode excitations in terms of the Cartesian quantum number v_z by counting the number of nodal planes perpendicular to the z axis. As for the translational excitations in the xy plane, Figs. 4 and 5, especially the latter, show unambiguously that for the purpose of assignment they can be viewed together as a two-dimensional (2D) isotropic HO. Its quantum numbers are (v,l), where v denotes the number of quanta and l is the vibrational angular momentum along the z axis; for a given v, l can take $v+1$ values, $-v,-v+2,\ldots,v-4,v-2,v$.[28] The values of l, actually the absolute values $|l|$, are determined by counting the number of angular nodes in the wave function perpendicular to the xy plane. Hence the complete translational quantum number assignment of a T-R level is $(v,|l|,v_z)$. When $|l|>0$, the level is doubly degenerate. Figures 6 and 7, which display the RPDs of the states $(2,|l|,1)$ ($|l|$=2,0) and (1,1,3), respectively, demonstrate the applicability of these translational quantum numbers to the T-R states where both the z mode and the 2D xy mode are excited, as well as the exceptional regularity of such T-R states. Evidently, the weak coupling between the translational mode parallel to the z axis and the two modes perpendicular to it persists at higher excitations.

The assignment of the translationally excited T-R levels of $H_2@C_{70}$ in terms of the quantum numbers $(v,|l|,v_z)$ is hardly unexpected. It is readily understood and indeed anticipated in view of (a) the high symmetry of the 5D PES in the xy plane and (b) the distinctly different potential profiles along the z axis and those along the x and y axes. Moreover, the same set of translational quantum numbers was identified already in our earlier quantum 3D calculations of the translational energy levels of the neon atom in C_{70}.[29] It was encountered also in our quantum 5D calculations of the T-R levels of H_2, HD, and D_2 in the small cage of sII clathrate hydrate.[13]

It should be pointed out that although the excitations of the 2D xy mode can be assigned with quantum numbers of

TABLE VIII. T-R energy levels of o-H_2 (v=1) inside C_{70} (in cm^{-1}) with *two* quanta in the 2D translational (xy) mode perpendicular to the long (z) axis of C_{70} from the quantum 5D calculations on the optimized PES. The excitation energies ΔE are relative to the T-R ground-state energy E_0=−1192.21 cm^{-1}. Other symbols have the same meaning as in Table V.

i	ΔE	g	Δx	Δy	Δz	$(v,\|l\|,v_z)$	j	$c(j)$
1	392.75	**2**	0.73	0.73	0.61	**(2,2,0)**	1	0.999
2	406.56	**2**	0.68	0.76	0.62	**(2,2,0)**	1	0.999
3	409.31	**2**	0.72	0.72	0.62	**(2,2,0)**	1	0.999
4	414.71	**1**	0.70	0.70	0.62	**(2,0,0)**	1	0.999
5	434.74	**2**	0.71	0.66	0.63	**(2,0,0)**	1	0.999

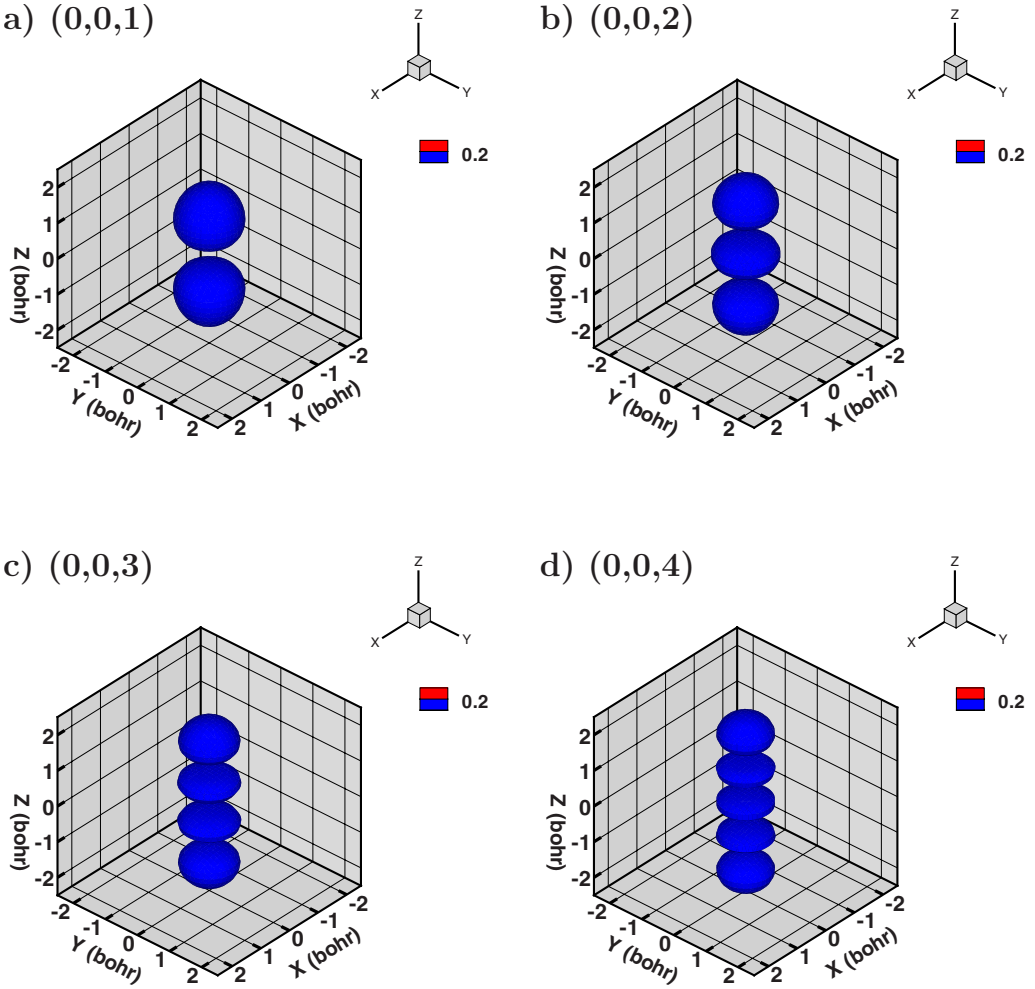

FIG. 3. (Color online) 3D isosurfaces of the RPD in the translational (Cartesian) coordinates of the $j=0$ T-R states $(0,0,v_z)$, $v_z=1-4$ of p-H_2 in C_{70} listed in Table V. The z axis is along the long axis of C_{70}. The isosurfaces are drawn at 20% of the maximum value of the density.

the 2D isotropic HO, they are definitely not harmonic. If they were, then their energies would depend on v only and not on l, i.e., they would be $(v+1)$-fold degenerate. However, Table V makes it clear that $(v,|l|,v_z)$ levels with the same v and v_z but different $|l|$ values have different energies. For example, the doubly degenerate level (2,2,0) has the energy of 293.45 cm^{-1}, while the level (2,0,0) is at 314.27 cm^{-1}. Consequently, the 2D xy mode is anharmonic. In fact, it shows *negative* anharmonicity, since the energy of the level (1,1,0) is 138.74 cm^{-1} and (2,2,0) level lies 154.71 cm^{-1} higher at 293.45 cm^{-1}. The z mode exhibits pronounced negative anharmonicity as well; the energy separation between the successive members of the pure z-mode progression $(0,0,v_z)$ increases with v_z from 77.72 cm^{-1} between (0,0,1) and (0,0,2) to 106.37 cm^{-1} between (0,0,3) and (0,0,4). Negative anharmonicity is typical for potentials with profiles such as those shown in Fig. 2(a). Thus, all translational modes of H_2 in C_{70} are characterized by negative anharmonicity.

The frequency of the z-mode fundamental (0,0,1), 54.15 cm^{-1}, is significantly lower than that of the 2D xy-mode fundamental (1,1,0), 138.74 cm^{-1}. This reflects the fact evident from Fig. 2 that the PES is noticeably stiffer in the direction of x and y axes than along the z axis. Greater translational freedom parallel to the z axis than in directions perpendicular to it is evident also from the rms amplitude Δz, which is considerably larger than Δx or Δy, for the same number of quanta in the z mode and the 2D xy mode, respectively. With the increasing number of quanta in the pure z mode $(0,0,v_z)$, Δz grows quite rapidly from 0.74 a.u. for (0,0,0) and 1.14 a.u. for (0,0,1) to 1.50 a.u. for (0,0,4).

2. Rotational excitations and translation-rotation coupling

So far, we have discussed only the translational excitations of H_2 (in the ground rotational state $j=0$) inside C_{70}. Our attention now turns to the rotational excitation of the caged H_2 and the very interesting issue of T-R coupling. First, we consider the $j=1$ and $j=2$ rotational levels of H_2 for the *ground* translational state (0,0,0). We find that their $(2j+1)$-fold degeneracy, which is fully preserved in C_{60},[16,17] is lifted in part by the angular anisotropy of the PES of $H_2@C_{70}$. Table VI and Fig. 8 show that the $j=1$ triplet of o-H_2 is split into a single state and a pair of degenerate states separated by 7.37 cm^{-1}. This is in accordance with the group theory,[30] which predicts that in the environment of D_{5h} symmetry the $j=1$ level splits into a nondegenerate and a doubly degenerate level [belonging to a_2'' (1D) and e_1' (2D) irreducible representations (IRs), respectively]. A complementary

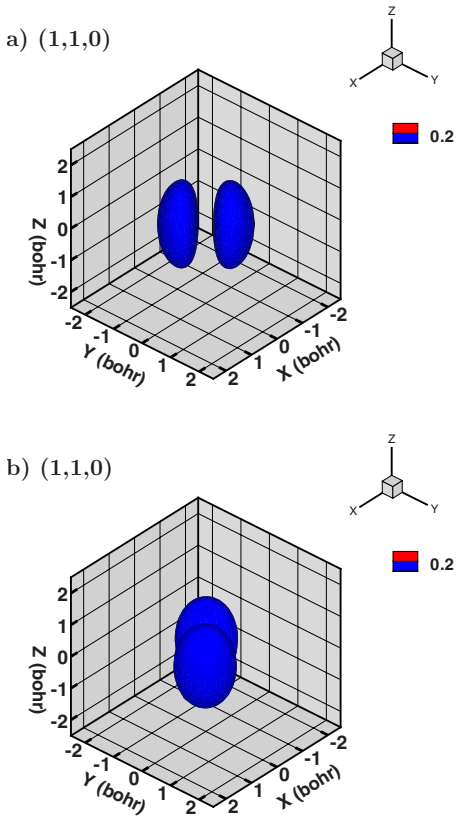

FIG. 4. (Color online) 3D isosurfaces of the RPD in the translational (Cartesian) coordinates of the pair of degenerate $j=0$ T-R states (1,1,0) of p-H_2 in C_{70} listed in Table V. The isosurfaces are drawn at 20% of the maximum value of the density.

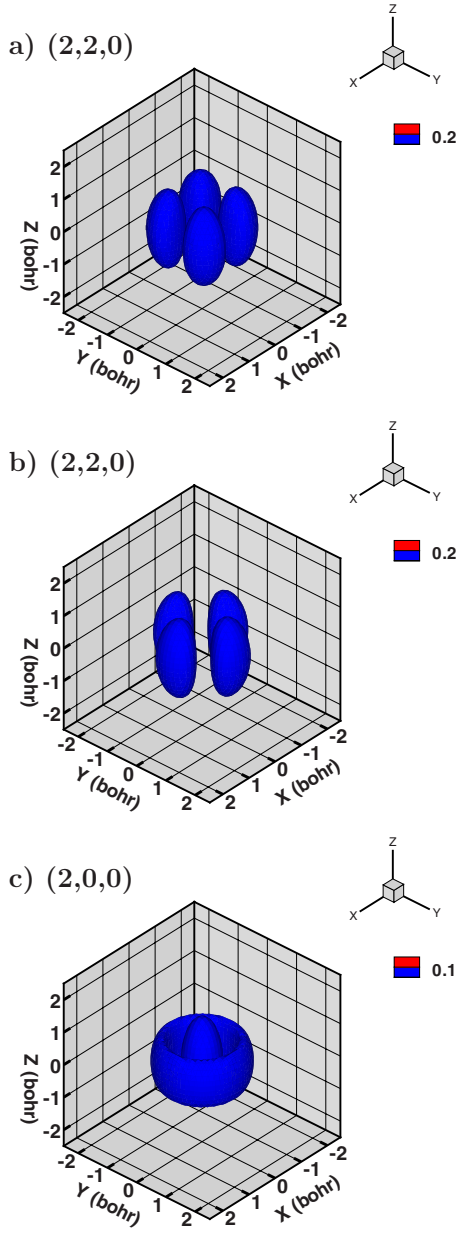

FIG. 5. (Color online) 3D isosurfaces of the RPD in the translational (Cartesian) coordinates of the three $j=0$ T-R states $(2,|l|,0)$ of p-H_2 in C_{70} with [(a) and (b)] $|l|=2$ and (c) $|l|=0$. They are listed in Table V. The isosurfaces are drawn at [(a) and (b)] 20% and (c) 10%, respectively, of the maximum value of the density.

and somewhat more physical view from the theoretical studies of H_2 in model SWCNTs[19,31] is that the nondegenerate level corresponds to H_2 oriented parallel to the z axis ($j=1$, $m=0$ state), while the doubly degenerate level is associated with H_2 transverse to the z axis ($j=1$, $m=\pm 1$ states). The $j=2$ level of p-H_2, which is fivefold degenerate in the gas phase, is split in a 1:2:2 degeneracy pattern evident in Table V and displayed in Fig. 9. Again, this curious splitting pattern can be understood with the help of the group theory, which predicts that the environment of D_{5h} symmetry splits the $j=2$ quintuplet into a nondegenerate level and two pairs of degenerate states [belonging to a_1' (1D), e_2' (2D), and e_1'' (2D) IRs, respectively]. The splitting between the nondegenerate and the closest doubly degenerate $j=2$ levels is only 0.18 cm^{-1}, and the second degenerate level lies 5.82 cm^{-1} higher.

Exciting the z mode alone does not change the above splitting patterns of the $j=1$ and $j=2$ levels, only the spacings between their components. For the $j=1$ level, the gap between the nondegenerate state and the degenerate doublet decreases with increasing v_z from 7.37 cm^{-1} for (0,0,0) to just 0.32 cm^{-1} for (0,0,4), as seen in Table VI and Fig. 8. The $j=2$ splitting pattern remains unchanged as well, but one quantum of excitation in the z mode increases the first splitting to 2.09 cm^{-1} and decreases the second slightly to 5.00 cm^{-1}; see Table V and Fig. 9.

Unlike the excitation of the z mode, one-quantum excitation of the 2D xy mode of o-H_2 ($j=1$) does result through T-R coupling in a new and intriguing pattern of T-R levels shown in Table VII and Fig. 10. The six states corresponding to $v=|l|=1$, $v_z=0$ and $j=1$ appear in the 2:1:2:1 pattern, which remains qualitatively the same upon exciting (also) the z mode, i.e., $v_z=1$ or 2. In the absence of the T-R coupling, these six states would be grouped in a degenerate pair and a degenerate quartet of states. Interestingly, the very same level pattern arises in what Yildirim and Harris[31] referred to as a "toy model" used to study the T-R coupling for the case of H_2 ($j=1$) molecule confined in a cylindrical potential, an idealized smooth representation of a SWCNT. Therefore, it seems that this particular energy level pattern is

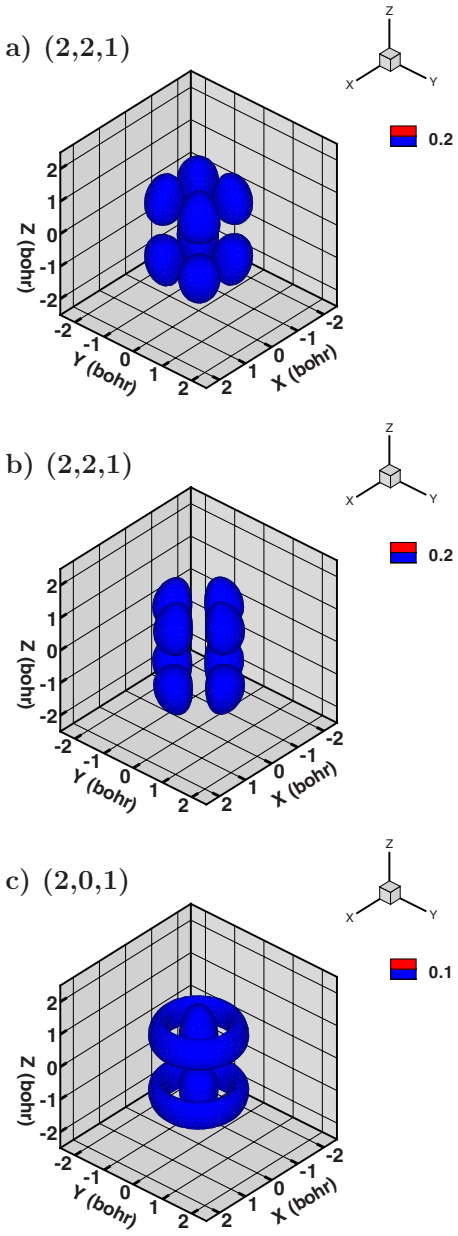

FIG. 6. (Color online) 3D isosurfaces of the RPD in the translational (Cartesian) coordinates of the three $j=0$ T-R states $(2,|l|,1)$ of p-H_2 in C_{70} with [(a) and (b)] $|l|=2$ and (c) $|l|=0$. They are listed in Table V. The isosurfaces are drawn at [(a) and (b)] 20% and (c) 10%, respectively, of the maximum value of the density.

obtained (for $v=|l|=1$ and $j=1$) whenever the confining potential has one axis which is distinct from the other two symmetrically equivalent axes perpendicular to it, regardless of whether H_2 is inside a nanotube or C_{70}.

Additional support for this comes from the analysis of the T-R states o-H_2 $(j=1)$ with *two* quanta in the 2D xy mode, i.e., $v=2$, $|l|=0,2$, $v_z=0$. Without the T-R coupling these nine states would appear as a degenerate triplet and a degenerate sextuplet. The T-R coupling gives rise to a peculiar 2:2:2:1:2 degeneracy pattern presented in Table VIII and Fig. 11. Qualitatively the same pattern of degeneracies was obtained for this case by Yildirim and Harris[31] in a highly simplified model of the T-R dynamics of H_2 in a cylindrical confinement.

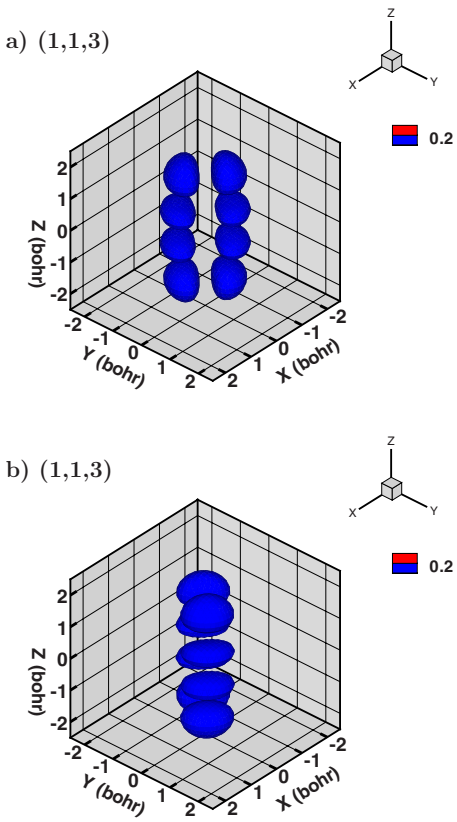

FIG. 7. (Color online) 3D isosurfaces of the RPD in the translational (Cartesian) coordinates of the pair of degenerate $j=0$ T-R states (1,1,3) of p-H_2 in C_{70} listed in Table V. The isosurfaces are drawn at 20% of the maximum value of the density.

IV. CONCLUSIONS

We have generated a quantitatively accurate pairwise additive 5D PES for H_2 in C_{60} by fitting to the recently published IR spectroscopic data[22] for this system, which characterize certain translational and rotational excitations of the confined H_2 in the vibrationally excited $v=1$ state. Our initial attempts in this direction using the standard description of the H_2–C interaction as the sum of two LJ H–C pair potentials (the two-site H_2–C pair potential) proved unsuccessful. Quantum 5D calculations of the T-R energy levels were unable to reproduce simultaneously the experimental values for the translational fundamental and the splittings between the three $n=1$, $j=1$ levels of o-H_2 in C_{60}, which arise from the T-R coupling. A major improvement was achieved by intro-

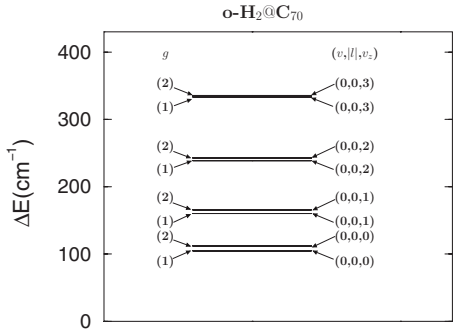

FIG. 8. Diagram of the T-R energy levels of o-H_2 $(j=1)$ in C_{70} with zero quantum in the 2D xy mode from Table VI.

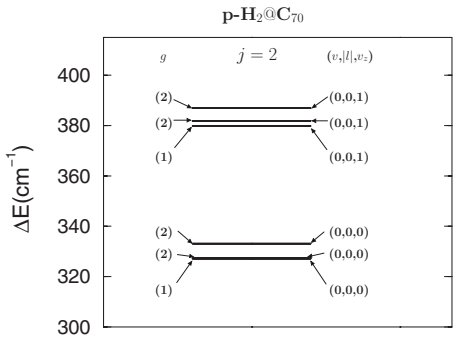

FIG. 9. Diagram of the T-R energy levels of p-H_2 (j=2) in C_{70} with zero quantum in the 2D xy mode from Table V.

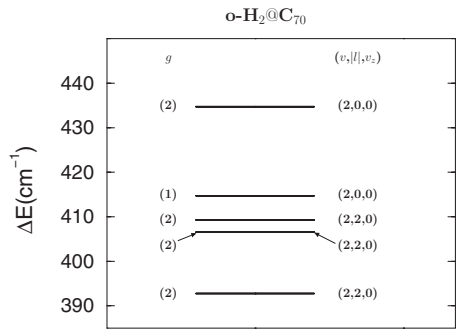

FIG. 11. Diagram of the T-R energy levels of o-H_2 (j=1) in C_{70} with two quanta in the 2D xy mode from Table VIII.

ducing the third LJ interaction site at the midpoint of the H–H bond in addition to the sites located on each H atom of H_2. We denoted this modified model of the H_2–C interactions as the three-site H_2–C pair potential. The pairwise additive 5D PES based on the three-site H_2–C pair potential has three adjustable parameters: ϵ_{HC}, σ_{HC}, and the weight w. A careful search of this 3D parameter space resulted in optimal values for which the additive 5D PES, when employed in the quantum 5D calculations, reproduces all six T-R energy levels observed in the IR spectra of $H_2@C_{60}$ to within 1–2 cm^{-1} (0.6%) or better. This demonstrated that a pairwise additive PES is capable of providing a quantitative description of the quantum T-R dynamics of H_2 inside C_{60}, provided that a suitable three-site H_2–C pair potential is used for its construction. In particular, the three-site H_2–C pair potential enables a much more realistic description of the angular anisotropy of the H_2-fullerene interaction than its two-site counterpart. The T-R energy levels computed on the optimized PES and reported in this paper will undoubtedly be helpful for the interpretation and assignment of the higher-temperature IR spectroscopic data on $H_2@C_{60}$ which should be available soon.[22] In turn, the new measurements will provide an additional test of the optimized PES and the three-site H_2–C potential developed here.

We are confident that the three-site model of the H_2–C pair interaction tested in the present work for H_2 in the ν=1 state will prove equally successful for constructing the pairwise additive 5D PES of H_2 in the ground vibrational state ν=0 once the relevant spectroscopic data for H_2 (ν=0) in C_{60} become available.

The three-site H_2–C pair potential spectroscopically optimized for $H_2@C_{60}$ was next used to construct the pairwise additive 5D PES for H_2 (ν=1) in C_{70}. Due to lower symmetry of C_{70} (D_{5h}) relative to that of C_{60} (I_h), the environment which the confined H_2 experiences is much more anisotropic than that felt inside C_{60}. The pronounced anisotropy of the 5D PES of H_2 in C_{70} with respect to the direction of the motion of the cm of the endohedral molecule gives rise to the T-R energy level structure which differs qualitatively from that elucidated by us previously for $H_2@C_{60}$ (Refs. 16 and 17) and requires an entirely different set of quantum numbers for its assignment. The translational excitations of H_2 in C_{70} were assigned in terms of the quantum numbers $(v,|l|,v_z)$, where v and l denote the number of quanta and the vibrational angular momentum parallel to the long (z) molecular axis of C_{70}, respectively, of the 2D isotropic harmonic HO in the plane of the two equivalent short (x and y) axes transverse to z, while v_z is the Cartesian quantum number for the 1D translational mode in the z direction. Both the 2D xy and the z translational modes exhibit significant negative anharmonicity. The j=1 and j=2 rotational levels of H_2 in C_{70} are partially split in 1:2 and 1:2:2 degeneracy patterns, respectively, already in the ground translational state, unlike in C_{60} where their $(2j+1)$-fold degeneracy is left intact. The level patterns which arise from the T-R coupling when H_2 is translationally excited, especially for one and two quanta in the 2D xy mode, are also totally unlike those computed for $H_2@C_{60}$.[16,17]

The T-R energy level structure of H_2 in C_{70} rigorously calculated for the first time in this work will serve as a guide to the experimentalists in their future spectroscopic studies of this prototypical anisotropic endohedral fullerene system. In addition, direct comparison with experimental results will constitute a stringent test of the degree to which the three-site H_2–C pair potential optimized for H_2 in C_{60} is transferable to another fullerene and ultimately to the interactions of H_2 with other nanocarbon materials. We have already performed the diffusion Monte Carlo calculations of the ground-state properties of two H_2 molecules inside C_{70} using the same H_2–C pair potential and a high-quality *ab initio* four-dimensional (rigid monomer) PES of the H_2 dimer; the results will be reported in a separate paper which is in preparation. Path integral Monte Carlo calculations will also be performed for this system in the near future in order to investigate the quantum T-R dynamics of two nanoconfined H_2 molecules as a function of temperature.

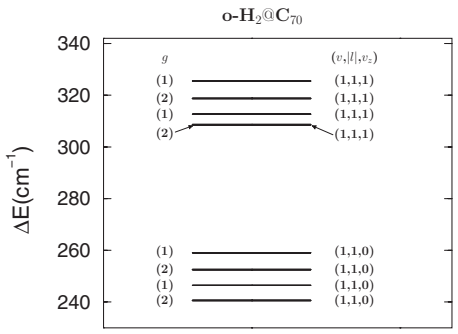

FIG. 10. Diagram of the T-R energy levels of o-H_2 (j=1) in C_{70} with one quantum in the 2D xy mode from Table VII.

ACKNOWLEDGMENTS

We thank the authors of Ref. 22 for early communication of the results prior to their publication. Z.B. is grateful to the National Science Foundation for partial support of this research through Grant No. CHE-0315508. The computational resources used in this work were funded in part by the NSF MRI Grant No. CHE-0420870. Acknowledgment is made to the donors of the American Chemical Society Petroleum Research Fund for partial support of this research. N.J.T. thanks the NSF for support of this research through Grant No. CHE-0717518.

[1] K. Komatsu, M. Murata, and Y. Murata, Science **307**, 238 (2005).
[2] M. Murata, Y. Murata, and K. Komatsu, J. Am. Chem. Soc. **128**, 8024 (2006).
[3] M. Murata, S. Maeda, Y. Morinaka, Y. Murata, and K. Komatsu, J. Am. Chem. Soc. **130**, 15800 (2008).
[4] Y. Rubin, T. Jarrosson, G. W. Wang, M. D. Bartberger, K. N. Houk, G. Schick, M. Saunders, and R. J. Cross, Angew. Chem., Int. Ed. **40**, 1543 (2001).
[5] E. Sartori, M. Ruzzi, N. J. Turro, J. D. Decatur, D. C. Doetschman, R. G. Lawler, A. L. Buchachenko, Y. Murata, and K. Komatsu, J. Am. Chem. Soc. **128**, 14752 (2006).
[6] M. Carravetta, A. Danquigny, S. Mamone, F. Cuda, O. G. Johannessen, I. Heinmaa, K. Panesar, R. Stern, M. C. Grossel, A. J. Horsewill, A. Samoson, M. Murata, Y. Murata, K. Komatsu, and M. H. Levitt, Phys. Chem. Chem. Phys. **9**, 4879 (2007).
[7] M. Carravetta, O. G. Johannessen, M. H. Levitt, I. Heinmaa, R. Stern, A. Samoson, A. J. Horsewill, Y. Murata, and K. Komatsu, J. Chem. Phys. **124**, 104507 (2006).
[8] Y. Murata, S. Maeda, M. Murata, and K. Komatsu, J. Am. Chem. Soc. **130**, 6702 (2008).
[9] J. Lopez-Gejo, A. A. Marti, M. Ruzzi, S. Jockusch, K. Komatsu, F. Tanabe, Y. Murata, and N. J. Turro, J. Am. Chem. Soc. **129**, 14554 (2007).
[10] E. Sartori, M. Ruzzi, N. J. Turro, K. Komatsu, Y. Murata, R. G. Lawler, and A. L. Buchachenko, J. Am. Chem. Soc. **130**, 2221 (2008).
[11] N. J. Turro, A. A. Marti, J. Y.-C. Chen, S. Jockusch, R. G. Lawler, M. Ruzzi, E. Sartori, S.-C. Chuang, K. Komatsu, and Y. Murata, J. Am. Chem. Soc. **130**, 10506 (2008).
[12] M. Xu, Y. Elmatad, F. Sebastianelli, J. W. Moskowitz, and Z. Bačić, J. Phys. Chem. B **110**, 24806 (2006).
[13] M. Xu, F. Sebastianelli, and Z. Bačić, J. Chem. Phys. **128**, 244715 (2008).
[14] F. Sebastianelli, M. Xu, and Z. Bačić, J. Chem. Phys. **129**, 244706 (2008).
[15] M. Xu, F. Sebastianelli, and Z. Bačić, J. Phys. Chem. A (in press).
[16] M. Xu, F. Sebastianelli, Z. Bačić, R. Lawler, and N. J. Turro, J. Chem. Phys. **128**, 011101 (2008).
[17] M. Xu, F. Sebastianelli, Z. Bačić, R. Lawler, and N. J. Turro, J. Chem. Phys. **129**, 064313 (2008).
[18] G. Garberoglio, M. M. DeKlavon, and J. K. Johnson, J. Phys. Chem. B **110**, 1733 (2006).
[19] T. Lu, E. M. Goldfield, and S. K. Gray, J. Phys. Chem. B **110**, 1742 (2006).
[20] S. J. V. Frankland and D. W. Brenner, Chem. Phys. Lett. **334**, 18 (2001).
[21] A. D. Novaco and J. P. Wroblievski, Phys. Rev. B **39**, 11364 (1989).
[22] S. Mamone, M. Ge, D. Hüvonen, U. Nagel, A. Danquigny, F. Cuda, M. C. Grossel, Y. Murata, K. Komatsu, M. H. Levitt, T. Rõõm, and M. Carravetta, J. Chem. Phys. **130**, 081103 (2009).
[23] K. Hedberg, L. Hedberg, D. S. Bethune, C. A. Brown, H. C. Dorn, R. D. Johnson, and M. de Vries, Science **254**, 410 (1991).
[24] A. V. Nikolaev, T. J. S. Dennis, K. Prassides, and A. K. Sopper, Chem. Phys. Lett. **223**, 143 (1994).
[25] S. Liu, Z. Bačić, J. W. Moskowitz, and K. E. Schmidt, J. Chem. Phys. **103**, 1829 (1995).
[26] Z. Bačić and J. C. Light, Annu. Rev. Phys. Chem. **40**, 469 (1989).
[27] V. Buch, J. Chem. Phys. **100**, 7610 (1994).
[28] L. D. Landau and E. M. Lifshitz, *Quantum Mechanics* (Pergamon, New York, 1977).
[29] M. Mandziuk and Z. Bačić, J. Chem. Phys. **101**, 2126 (1994).
[30] F. A. Cotton, *Chemical Application of Group Theory*, 2nd ed. (Wiley-Interscience, New York, 1970).
[31] T. Yildirim and A. B. Harris, Phys. Rev. B **67**, 245413 (2003).